MOLECULAR PHYSICS, 10–20 OCTOBER 2004, VOL. 102, NO. 19–20, 2149–2163

Taylor & Francis
Taylor & Francis Group

Freezing and melting of binary mixtures confined in a nanopore

BENOIT COASNE[1], JOANNA CZWARTOS[2], KEITH E. GUBBINS[1]*, FRANCISCO R. HUNG[1] and MALGORZATA SLIWINSKA-BARTKOWIAK[2]

[1]Department of Chemical Engineering, North Carolina State University, Raleigh, NC 27695-7905, USA
[2]Institute of Physics, Adam Mickiewicz University, Umultowska 85, 61-614 Poznan, Poland

(*Received 25 March 2004; accepted 21 July 2004*)

This paper reports on a Grand Canonical Monte Carlo study of the freezing and melting of Lennard–Jones Ar/Kr mixtures confined in a slit pore composed of two strongly attractive structureless walls. For all molar compositions and temperatures, the pore, which has a width of 1.44 nm, accommodates two contact layers and one inner layer. Different wall/fluid interactions are considered, corresponding to pore walls that have a larger affinity for either Ar or Kr. The solid/liquid phase diagram of the confined mixture is determined and results compared with data for the bulk mixture. The structure of the confined mixture is studied using 2D order parameters and both positional $g(r)$ and bond orientational $G_6(r)$ pair correlation functions. It is found that in the confined solid phase, both the contact and inner layers have a hexagonal crystal structure. It is shown that the freezing temperature of the Ar/Kr confined mixture is higher than the bulk freezing point for all molar compositions. Also, it is found that the freezing temperature becomes larger as the ratio α of the wall/fluid to the fluid/fluid interactions increases, in agreement with previous simulation studies on pure substances confined in nanopores. In the case of pore walls having a stronger affinity for Kr atoms ($\varepsilon_{Ar/W} < \varepsilon_{Kr/W}$), it is observed that both the contact and inner layers of the confined mixture undergo, at the same temperature, a transition from the liquid phase to the crystal phase. The freezing of Ar/Kr mixtures confined between the walls having a stronger affinity for Ar ($\varepsilon_{Ar/W} > \varepsilon_{Kr/W}$) is more complex: for Kr molar concentration lower than 0.35, we observe the presence of an intermediate state between all layers being 2D hexagonal crystals and all the layers being liquid. This intermediate state consists of a crystalline contact layer and a liquid-like inner layer. It is also shown that the qualitative variations of the increase of freezing temperature with the molar composition depend on the affinity of the pore wall for the different components. These results confirm that, in addition to the parameter α the ratio of the wall/fluid interactions for the two species, $\eta = \varepsilon_{Ar/W}/\varepsilon_{Kr/W}$, is a key variable in determining the freezing and melting behaviour of the confined mixture.

1. Introduction

Freezing and melting of pure substances confined in nanopores have been extensively studied using both experiments and molecular simulations (for reviews see [1–3]). In addition to its fundamental interest, understanding the effect of confinement on melting and freezing phenomena is important in many applications, including lubrication, fabrication of structured nanomaterials, nanotribology and adhesion. In contrast to the case of pure substances, there seems to have been no studies of freezing and melting of confined mixtures of simple fluids; a few studies of a molten salt and colloidal mixture have been reported [4–6]. Using high resolution transmission electronic microscopy, Meyer *et al.* [4] have shown that the freezing of potassium iodide confined in a 1.6 nm single wall carbon nanotube occurs at a temperature significantly larger than the bulk freezing point. Moreover, the lattice spacing of the confined solid was found to be different to that of the bulk crystal [4]. Wilson [5] compared the experimental data obtained by Meyer *et al.* with molecular simulations for confined potassium iodide and found that the radius of the carbon nanotube has a crucial effect on the formation of the confined crystal. Recently, Cui *et al.* [6] studied the freezing behaviour of confined mixtures composed of large and small spherical colloids. The authors showed

*Author for correspondence. e-mail: keg@ncsu.edu

Molecular Physics ISSN 0026–8976 print/ISSN 1362–3028 online
http://www.tandf.co.uk/journals
DOI: 10.1080/00268970412331292678

that the liquid density at the freezing transition is strongly dependent on both the density of small spheres and the diameter ratio of the colloidal particles. In this paper, we report the first simulation study of the effects of confinement and of the wall/fluid interactions on freezing and melting transitions of simple Lennard–Jones mixtures confined in a slit pore. The fluid/fluid interaction parameters are chosen to model an argon/krypton mixture. As in the case of pure substances [7], the pore width H and the parameter α, defined as the ratio of the wall/fluid to the fluid/fluid attractive interactions, are expected to play an important role in the melting and freezing behaviour of the mixture. In addition, for binary mixtures the parameter $\eta = \varepsilon_{\mathrm{Ar/W}}/\varepsilon_{\mathrm{Kr/W}}$, defined as the ratio of the wall/fluid interaction for the two species, should also be a key parameter in describing the freezing. Finally, the temperature of the freezing transition should depend on the molar composition of the mixture, as in the case of the bulk system [8, 9].

In this paper, we report Grand Canonical Monte Carlo (GCMC) simulations of the freezing of mixtures confined in a structureless slit pore of width $H = 1.44$ nm, having graphitic walls. Fluid/fluid interaction parameters are chosen to mimic argon/krypton mixtures [9]. We consider different wall/fluid interactions and study mixtures confined between pore walls having either a larger affinity for Ar ($\eta > 1$) or Kr ($\eta < 1$). For both types of pore material, we discuss the confinement effect on the freezing temperature and its dependence on the molar composition of the mixture. We also determine the solid/liquid phase diagram of the confined system and compare our results with data available for the bulk mixture. Finally, the structure of the confined phase is studied by calculating 2D bond order parameters, and both positional and bond orientational pair correlation functions. The paper is organized as follows. In section 2, we present the details of the simulation study and give a short description of the numerical techniques. In section 3, we present and discuss results for the freezing and melting of Ar/Kr mixtures confined in the 1.44 nm slit pore for the different wall/fluid interactions. In section 4, we summarize our results and suggest future works. We are pleased to contribute this paper in honour of Jack G. Powles on the occasion of his eightieth birthday. Among his numerous scientific works, Jack G. Powles made significant contributions to the field of confined fluids [10–14] and liquid mixtures [15–18].

2. Computational details

2.1. *Grand Canonical Monte Carlo*

The GCMC technique consists of determining the properties of a system having a constant volume V (the pore with the confined phase) in equilibrium with an infinite fictitious reservoir of particles imposing its chemical potential for each species μ_{Ar}, μ_{Kr} and its temperature T [19–21]. The state i of the system can be defined by its energy U^i and the numbers N^i_{Ar}, N^i_{Kr} of Ar and Kr atoms. The GCMC algorithm is based on the generation of a Markov chain of states that are obtained by creating a particle at a random position, deleting or displacing an existing particle. In the case of mixtures, we add a fourth move that consists of exchanging the identity of an existing particle [22]. In the framework of the Metropolis algorithm scheme, the acceptance probability P_{acc} for the identity exchange of a particle i into a particle j ($i, j =$ Ar or Kr) is given by [21]:

$$P_{acc} = \min\left(1, \frac{N_i Z_j}{(N_j + 1) Z_i} \exp(-\beta \Delta U)\right), \qquad (1)$$

where ΔU is the change in configurational energy resulting from the move, while Z_i is the absolute activity of species i. In order to circumvent the difficulty of particle deletion and insertion in dense phases such as liquids and solids, we have included in our GCMC simulations a parallel tempering technique [21, 23, 24]. This method consists of considering several replicas (R) of the system at different temperatures $T^{(\mathrm{R})}$ and chemical potentials $\mu^{(\mathrm{R})}_{\mathrm{Ar}}$, $\mu^{(\mathrm{R})}_{\mathrm{Kr}}$. For each replica, conventional Monte Carlo moves are attempted. In addition, trial swap moves between the configuration A ($U^A, N^{\mathrm{A}}_{\mathrm{Ar}}, N^{\mathrm{A}}_{\mathrm{Kr}}$) of a replica (1) and the configuration B ($U^{\mathrm{B}}, N^{\mathrm{B}}_{\mathrm{Ar}}, N^{\mathrm{B}}_{\mathrm{Kr}}$) of a replica (2) are attempted. The swap is accepted or rejected according to a probability defined in the framework of the Metropolis algorithm [21, 23]:

$$P_{acc} = \min\left(1, \frac{\exp(-\beta^{(2)} U^A) \exp(-\beta^{(1)} U^B)}{\exp(-\beta^{(1)} U^A) \exp(-\beta^{(2)} U^B)} \times \prod_i \exp -(\beta^{(2)} \mu_i^{(2)} - \beta^{(1)} \mu_i^{(1)})(N_i^B - N_i^A)\right) \qquad (2)$$

where the product is for $i =$ Ar and Kr. The parallel tempering technique improves the sampling of phase space and prevents the system from being 'trapped' in local metastable states [25, 26]. The number of replicas used in our simulation is 16 and the temperature difference between two successive replicas is $\Delta T = 2$ K. In this work, a MC step corresponds to a particle displacement attempt and either a deletion or a creation attempt. In addition, identity exchanges and configuration swaps (parallel tempering) are attempted every 5 and 20 000 MC steps, respectively. The number of particles in each replica is about 300–400. In order to study freezing, we started with a liquid system and first performed 400×10^6 Monte Carlo steps to equilibrate

Table 1. Lennard–Jones parameters used to calculate the fluid/fluid interactions.

Ar/Ar	$\sigma = 0.3336\,\text{nm}$	$\varepsilon = 141.2\,\text{K}$
Kr/Kr	$\sigma = 0.3575\,\text{nm}$	$\varepsilon = 191.4\,\text{K}$
Ar/Kr	$\sigma = 0.3456\,\text{nm}$	$\varepsilon = 164.4\,\text{K}$

the system. After equilibration of the system, density profiles, bond order parameters, and pair correlation functions were averaged in the course of a second simulation run of 400×10^6 Monte Carlo steps. The final solid configuration at the lowest temperature was then used as the starting point for the study of the melting process, which proceeds in an analogous way to freezing.

2.2. *Intermolecular potential functions*

In this work, we studied the freezing behaviour of Ar/Kr mixtures confined in a slit pore. The pore width was $H = 1.44\,\text{nm}$ ($\sim 4.3\sigma$, σ being the size of the argon atom) and the size of the square section was $3.6 \times 3.6\,\text{nm}$ ($\sim 10\sigma \times 10\sigma$). Periodic boundary conditions were applied in the directions (x, y) parallel to the pore walls. The fluid/fluid interactions Ar/Ar and Kr/Kr were calculated using Lennard–Jones potentials with the parameters shown in table 1 [9, 27]. The cross-species Ar/Kr Lennard–Jones parameters were calculated using the Lorentz–Berthelot combining rules [28].

The slit pore is described as an assembly of two structureless parallel walls and the fluid/wall interaction is calculated using the Steele '10-4-3' potential [29, 30]:

$$U_{wf}(z) = 2\pi\rho_w\varepsilon_{wf}\sigma_{wf}^2\Delta \times \left[\frac{2}{5}\left(\frac{\sigma_{wf}}{z}\right)^{10} - \left(\frac{\sigma_{wf}}{z}\right)^4 - \left(\frac{\sigma_{wf}^4}{3\Delta(z+0.61\Delta)^3}\right)\right], \tag{3}$$

where z is the distance between the adsorbed molecule and the graphite surface. Δ is the separation between graphite layers, 0.335 nm, and ρ_w the atomic density of graphite layers, $114\,\text{nm}^{-3}$, while ε_{wf} and σ_{wf} are the wall/fluid Lennard–Jones parameters. The first and second terms in equation (1) are respectively the repulsive and attractive parts of the interaction between the adsorbed molecule and the graphite surface while the third term represents the summation over the other graphite layers. In the case of a slit pore having a width H, the fluid interacts with both graphite surfaces and the total fluid/wall interaction is given by:

$$V_{wf}(z) = U_{wf}(z) + U_{wf}(H - z), \tag{4}$$

Table 2. Lennard–Jones parameters used to calculate the two different wall/fluid interactions (A) and (B). α is the ratio of the wall/fluid to the fluid/fluid interactions (see equation (5)), while $\eta = \varepsilon_{\text{Ar/W}}/\varepsilon_{\text{Kr/W}}$.

(A)	Ar/W	$\sigma = 0.3368\,\text{nm}$	$\varepsilon = 62.9\,\text{K}$	$\alpha = 1.93$	$\eta = 0.86$
	Kr/W	$\sigma = 0.3488\,\text{nm}$	$\varepsilon = 73.2\,\text{K}$	$\alpha = 1.78$	
(B)	Ar/W	$\sigma = 0.3368\,\text{nm}$	$\varepsilon = 78.2\,\text{K}$	$\alpha = 2.40$	$\eta = 1.07$
	Kr/W	$\sigma = 0.3488\,\text{nm}$	$\varepsilon = 73.2\,\text{K}$	$\alpha = 1.78$	

where $U_{wf}(z)$ and $U_{wf}(H - z)$ are calculated using equation (3).

Two different wall/fluid interactions (A) and (B), with different sets of ε_{wf} and σ_{wf} values, were studied throughout this work. The first set of parameters (A) was determined by combining the wall/wall and fluid/fluid Lennard–Jones parameters using the Lorentz–Berthelot rules (see table 2). The values $\varepsilon_{ww} = 28\,\text{K}$ and $\sigma_{ww} = 0.34\,\text{nm}$ were used for the Lennard–Jones parameters for the carbon wall [30]. The wall/fluid interaction parameters for this first set (A) mimic interactions of Ar and Kr atoms with graphitic walls in a realistic way. Given that $\varepsilon_{\text{Kr/Kr}}$ is larger than $\varepsilon_{\text{Ar/Ar}}$, the use of the Lorentz–Berthelot combining rules leads to a Kr/wall interaction that is stronger than the Ar/wall interaction $\varepsilon_{\text{Ar/W}} < \varepsilon_{\text{Kr/W}}$ ($\eta = \varepsilon_{\text{Kr/W}}/\varepsilon_{\text{Kr/W}} < 1$). This is expected for real Ar/Kr confined mixtures since the wall/fluid interaction for a rare gas atom is proportional to its polarizability, which increases with the atomic number of the species. For the second set of wall/fluid interactions (B), we considered a mixture with Ar/wall interactions larger than the Kr/wall interactions ($\eta > 1$). We change arbitrarily the energy parameter $\varepsilon_{\text{Ar/W}}$ from 62.9 K (parameter set A) to 78.2 K (parameter set B). In contrast, the parameter $\varepsilon_{\text{Kr/W}} = 73.2\,\text{K}$ is chosen identical to that for interactions (A) (see table 2). We note that this second choice of interaction parameters (B) does not correspond to realistic Ar/Kr confined mixtures. However, the comparison between results for the interaction parameters (A) and (B) allows us to study the effect of the affinity of the pore wall on the freezing behaviour for confined mixtures corresponding to the same fluid/fluid interactions and, therefore, the same bulk phase diagram.

Following previous works [7, 31], we define for both Ar and Kr the parameter α that accounts for the ratio of the wall/fluid to the fluid/fluid interactions (see equation (1)):

$$\alpha = \rho_w\varepsilon_{wf}\,\sigma_{wf}^2\Delta/\varepsilon_{ff} \tag{5}$$

Using a corresponding states analysis [32], Radhakrishnan *et al.* [7, 31] have shown that, for a given reduced pore width $H^* = H/\sigma$, the change in

freezing temperature of a confined system can be related to the α parameter. Using the interactions parameters (A) and (B), the values of α for Ar are $\alpha_{Ar}=1.93$ and $\alpha_{Ar}=2.40$, respectively (see table 2). On the other hand, the parameter $\alpha_{Kr}=1.78$ is identical for both the interactions (A) and (B). We expect the freezing temperature of the confined mixture to be larger than that of the bulk since previous experimental [33–37] and simulation [7, 31, 38] works have shown that pure fluids confined in strongly attractive pores with $\alpha > 1$ undergo a transition from a liquid-like to a solid-like structure at temperatures above the bulk freezing point.

2.3. *Simulation parameters*

The constant parameters of a GCMC simulation are the chemical potentials μ_{Ar}, μ_{Kr} and the temperature T that are imposed by the infinite reservoir of particles. The relations $\mu_{Ar}(T)$ and $\mu_{Kr}(T)$ were extracted from the bulk phase diagram (see figure 1) that has been calculated by Hitchcock and Hall [9] using the Gibbs–Duhem integration method [39–41]. This phase diagram (T, x_{Kr}) at constant pressure $p=1$ atm gives the krypton mole fraction x_{Kr} of the coexisting liquid and solid states as a function of the solid/liquid transition temperature T_f^0 at a pressure of 1 atm. The Gibbs–Duhem integration method has been shown to reproduce the shape of the experimental phase diagram for several mixtures [42–44]. In the case of Ar/Kr mixtures at a pressure $p \sim 1$ atm [9], the shape of the phase diagram predicted by Hitchcock and Hall is of the type 'solid solution', in agreement with Heastie's experiments [8]. The freezing temperature is a monotonous increasing function of the Kr mole fraction and varies from the bulk freezing point of pure Ar, $T=97.3$ K, to that of pure Kr, $T=131.9$ K.

The chemical potentials $\mu_{Ar}(T)$, $\mu_{Kr}(T)$ were calculated from the phase diagram of the bulk mixture using the following equation proposed by Mehta and Kofke [45]:

$$d\ln(f_1+f_2) - h_r d\beta + Z d\ln p - \frac{x_2-\xi_2}{\xi_2(1-\xi_2)}d\xi_2, \qquad (6)$$

where f_1, f_2 are the fugacities of components 1 and 2, h_r the residual molar enthalpy, Z the compressibility factor and p the pressure; x_2 and ξ_2 are the mole and fugacity fractions of component 2. The chemical potential of component i is related to its fugacity *via* $f_i = \exp(\beta\mu_i)$. Equation (6) was integrated using the Simpson method [46] and starting from the fugacity of pure Kr at its melting point. In order to check the validity of the relations $\mu_{Ar}(T)$, $\mu_{Kr}(T)$ that we extracted, we performed GCMC simulations for bulk Ar/Kr mixtures in the liquid phase and compared our results with the bulk phase diagram (see figure 1). The GCMC data are in good agreement with results obtained by Hitchcock and Hall [9].

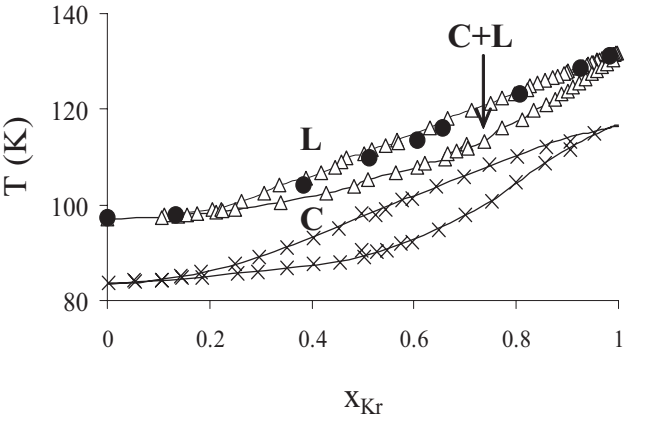

Figure 1. (T, x_{Kr}) solid–liquid phase diagram for an Ar/Kr bulk mixture at a constant pressure $p=1$ atm. Open triangles are data obtained using the Gibbs–Duhem integration method (from Hitchcock and Hall [9]); crosses are Heastie's experiments [8]. Closed circles are GCMC simulations (see text). In the theoretical phase diagram, C and L denote the crystal and liquid regions respectively. Lines are to guide the eye.

2.4. *2D order parameter and pair correlation functions*

The structure of the confined mixture was investigated by means of 2D bond order parameters and both positional and bond orientational pair correlation functions. Following previous simulation studies [7, 47], we determined the local order parameter $\Psi_{6,j}(\mathrm{r})$ that measures the hexagonal bond order at a position r of a particle located in the layer j [7, 47, 48]:

$$\Psi_{6,j}(\mathbf{r}) = \frac{1}{N_b}\sum_{k=1}^{N_b}\exp(i6\theta_k) \qquad (7)$$

where θ_k are the bond angles between the particle and each of its N_b nearest neighbours. For each layer j of the confined mixture, the 2D bond order parameter $\Phi_{6,j}$ is defined from the average value of the local order parameter over the layer:

$$\Phi_{6,j} = \frac{\left|\int \Psi_{6,j}(\mathbf{r})\mathrm{d}\mathbf{r}\right|}{\mathrm{d}\mathbf{r}} \qquad (8)$$

$\Phi_{6,j}$ is expected to be close to 1 for a layer having a hexagonal structure and close to 0 for a layer having a liquid-like structure.

For each layer j of the confined mixture, the 2D positional pair correlation function $g(r)$ was used to determine whether the layer exhibits long range (solid-like)

or short range (liquid-like) positional order. Following the work of Miyahara and Gubbins [38], the $g(r)$ function for each layer was calculated from the GCMC configuration as:

$$g(r) = \frac{N(r, z_j, z_{j-1})}{2\pi r \Delta r \rho_j} \tag{9}$$

where $N(r, z_j, z_{j-1})$ is the number of particles at a distance between $r - (\Delta r/2)$ and $r + (\Delta r/2)$ from a reference molecule, in the layer j bounded by z_{j-1} and z_j. We note that the distance r is the projection of the pair separation parallel to the pore walls. The normalization factor in equation (9) corresponds to the number of particles of an ideal gas having the density ρ_j of the layer j that would be comprised in the surface area $2\pi r \Delta r$.

We also monitored for each layer j the 2D bond orientational pair correlation function $G_6(r)$. This function measures the correlations between the local bond order parameter $\Psi_{6,j}(r)$ at two positions separated by a distance r:

$$G_6(r) = \langle \Psi^*_{6,j}(0) \Psi_{6,j}(r) \rangle. \tag{10}$$

The real part of $G_6(r)$ is the amplitude of the bond orientational order, while the imaginary part gives the phase of the layer, i.e. the alignment direction of the hexagonal crystal. In the case of this work, we are dealing with single crystal layers so that the imaginary part is negligible. Therefore, only the real part of $G_6(r)$ is reported in what follows. The pair correlation function $G_6(r)$ can be used to assess the structure of the confined phase: hexagonal crystal, hexatic phase or liquid phase. In the case of a 2D crystal having a hexagonal structure, the layer exhibits long range bond orientational order and, consequently, $G_6(r)$ has a constant, finite value even at large distances. For a layer having a liquid-like structure, there is no bond orientational order and $G_6(r)$ is an exponentially decaying function of r. A hexatic phase is characterized by a quasi-long range bond orientational order (without positional order) and $G_6(r)$ decays algebraically with r.

3. Results and discussion

3.1. *Ar/Kr mixtures confined in a slit pore having a stronger affinity for Kr*

In this section, we first discuss the freezing and melting of Ar/Kr mixtures using the wall/fluid energy parameters (A); the α parameters for Ar and Kr are respectively 1.93 and 1.78 and the ratio of the Ar/wall to the Kr/wall interaction is $\eta = \varepsilon_{Ar/W}/\varepsilon_{Kr/W} = 0.86$.

3.1.1. *Properties of the confined mixture*

Using the simulation parameters $\mu_{Ar}(T)$ and $\mu_{Kr}(T)$ obtained from the bulk phase diagram shown in figure 1, we first simulated confined Ar/Kr mixtures in equilibrium with infinite bulk mixtures at solid/liquid coexistence conditions. Figure 2 shows the ratio of the Kr mole fraction inside the pore to that of the bulk mixture for temperatures varying from the bulk freezing point at $p = 1$ atm of pure Ar, $T_f^0 \sim 97$ K, up to that of pure Kr, $T_f^0 \sim 131$ K. For all temperatures, the confined mixture has a larger Kr molar concentration than the bulk mixture. This result is in agreement with previous simulation [22] and theoretical [49] works for ethane/methane liquid mixtures confined in a slit graphitic pore, which have shown that the molar composition of the component having the strongest interaction with the pore wall is increased compared to the bulk.

Density profiles $\rho(Z^*)$ of the confined Ar/Kr mixture are shown in figure 3 for different temperatures and molar compositions of the bulk solid/liquid coexistence at $p = 1$ atm. Z^* is the distance from the centre of the slit pore in reduced units with respect to the Lennard–Jones parameter σ_{Ar}. Simulation snapshots corresponding to the different density profiles are also shown in figure 4. The density profiles for the highest temperatures $T = 104.1$ K ($x_{Kr} = 0.82$) and $T = 97.9$ K ($x_{Kr} = 0.43$) are very similar: the confined mixture has a layered structure composed of two contact layers and one inner layer. The density profile for the lowest temperature $T = 97.3$ K ($x_{Kr} = 0.00$) also exhibits three layers. However, the peak corresponding to the inner layer for this temperature and molar composition is split into two secondary peaks located at $Z^* = 0.14$ and

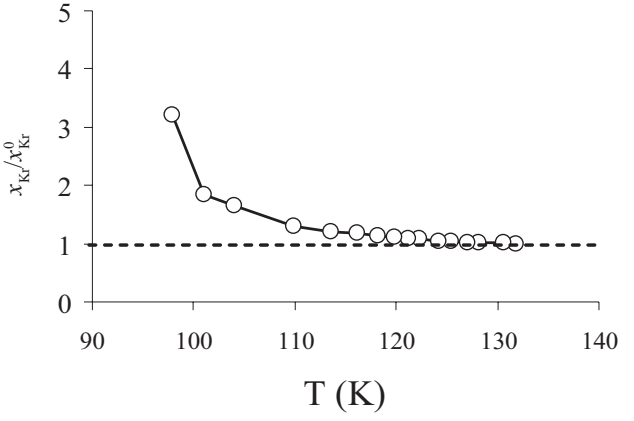

Figure 2. Ratio of the Kr mole fraction x_{Kr} inside the 1.44 nm slit pore ($\alpha_{Ar} = 1.93$, $\alpha_{Kr} = 1.78$, $\eta = 0.86$), to that of the bulk system x^0_{Kr} for temperatures corresponding to the bulk solid/liquid coexistence at $p = 1$ atm (T varies from the bulk freezing point of pure Ar, ~97 K, up to that of pure Kr, ~131 K).

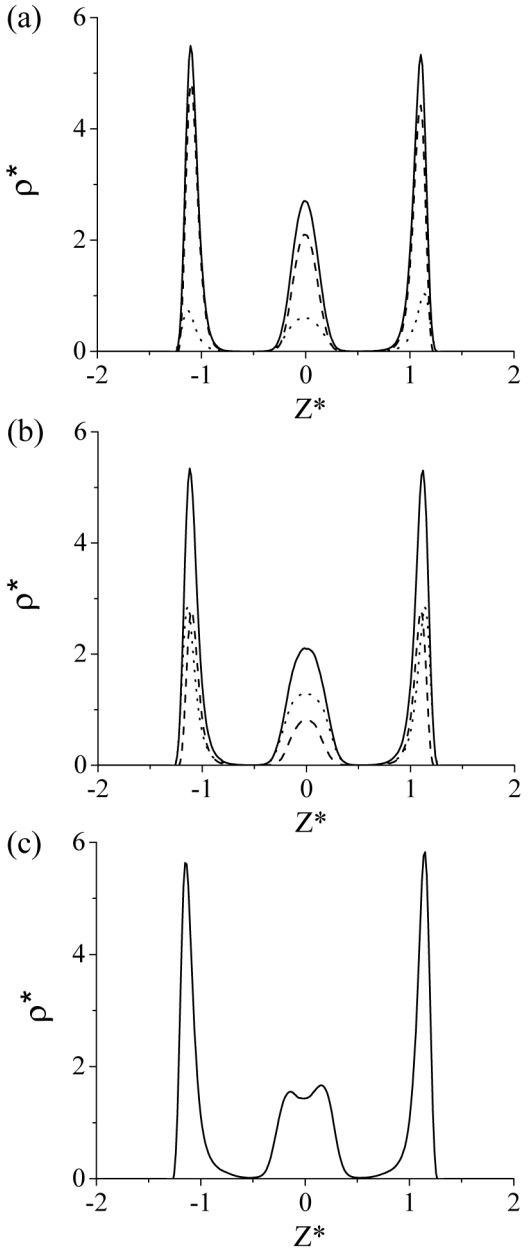

Figure 3. Density profiles of Ar/Kr mixtures confined in the 1.44 nm slit pore, with $\alpha_{Ar} = 1.93$, $\alpha_{Kr} = 1.78$, $\eta = 0.86$, at different temperatures of the bulk solid/liquid coexistence: (*a*) $T = 104.1$ K, (*b*) $T = 97.9$ K and (*c*) 97.3 K (the freezing point of pure Ar). The Kr mole fraction inside the pore is (*a*) $x_{Kr} = 0.82$, (*b*) $x_{Kr} = 0.43$ and (*c*) $x_{Kr} = 0.00$. Full line is total density profile while dotted and dashed lines are Ar and Kr contributions, respectively. Z^* is the distance from the centre of the pore in reduced units with respect to σ_{Ar}. Figure (*c*) has only one line since this case $T = 97.3$ K corresponds to pure Ar.

$Z^* = -0.14$. This type of layered structure, referred as a 'buckled phase' in the literature, is an intermediate stable state that results from structural transitions of the confined phase (change of crystal symmetry, increase in the number of layers) [50]. This buckled layer cannot be seen as two different layers of the confined mixture since the distance that separates the secondary peaks $\sim 0.28\sigma_{Ar}$ is much lower than the diameter of the particles. Moreover, the minimum value of the density between the two secondary peaks, $\rho(Z^*) \sim 1.45$, is large compared to that between the inner layer and the contact layer, $\rho(Z^*) \sim 0.01$.

We have also reported in figure 3 the different contributions $\rho_{Ar}(Z^*)$ and $\rho_{Kr}(Z^*)$ that were calculated by distinguishing the Ar and Kr atoms. For both the contact and inner layers, the ratio of the peak amplitude to the peak width for Kr is larger than that for Ar. This result shows that, due to their larger size, Kr atoms are more strongly localized within each layer than Ar atoms. We also found that the Kr mole fraction inside the contact layer is larger than inside the inner layer. This result shows that, due to their stronger interaction with the pore wall ($\varepsilon_{Kr/W} > \varepsilon_{Ar/W}$), Kr atoms are preferentially adsorbed close to the pore wall, *i.e.* within the contact layer.

In order to determine the structure of the confined phase, we calculated the 2D positional pair correlation function $g(r)$ for the contact and inner layers. The boundaries of each layer were determined as the locations at which the local density $\rho(Z^*)$ exhibits minima (see figure 3) [51]. In figure 5, we show $g(r)$ functions obtained for different temperatures/molar compositions corresponding to the bulk solid/liquid coexistence at a pressure of 1 atm. For the sake of clarity, the $g(r)$ functions for the contact layer have been shifted by $+2$. These positional pair correlation functions were calculated without distinguishing Ar and Kr atoms. However, we checked that the contributions $g_{Ar/Ar}(r)$, $g_{Ar/Kr}(r)$ and $g_{Kr/Kr}(r)$ were identical to the total $g(r)$ function. This result suggests that each layer of the adsorbate is in a miscible phase. As can be seen in figure 5, both the contact and the inner layers have a solid-like structure for all temperatures and molar compositions. Indeed, the 2D positional pair correlation functions $g(r)$ exhibit the following features that are characteristic of a crystal phase: (i) the amplitude in between the first and the second peak is close to 0; (ii) the second peak is split into two secondary peaks; and (iii) the third peak presents a shoulder on its right side. Although these properties are more pronounced for the layer close to the pore wall, the $g(r)$ function for the inner layer is almost identical to that obtained for the contact layer. This result is in good agreement with previous results obtained by Radhakrishnan *et al.* [52] showing that, for pores accommodating three layers, the contact and inner layers behave similarly upon freezing. As will be discussed in detail below, we found that the solid

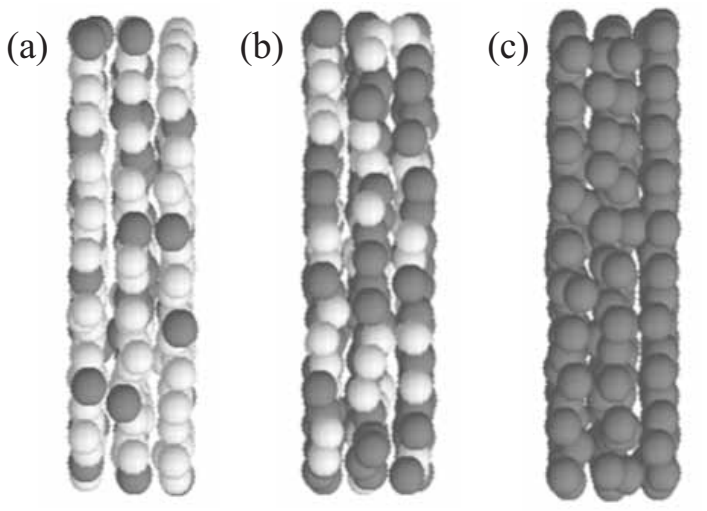

Figure 4. Simulation snapshots of Ar/Kr mixtures confined in the 1.44 nm slit pore, $\alpha_{Ar} = 1.93$, $\alpha_{Kr} = 1.78$, $\eta = 0.86$, corresponding to density profiles shown in figure 3: (*a*) $T = 104.1$ K, $x_{Kr} = 0.82$, (*b*) $T = 97.9$ K, $x_{Kr} = 0.43$ and (*c*) $T = 97.3$ K, $x_{Kr} = 0.00$. Gray and white spheres correspond to Ar and Kr atoms respectively.

confined mixture corresponds to crystal layers having a hexagonal structure in which each atom is surrounded by six nearest neighbours belonging to the same layer.

The solid-like structure of the confined Ar/Kr mixtures, at conditions of the bulk liquid/solid coexistence, shows that the in-pore freezing temperatures, $T(x_{Kr})$, are equal or superior to their bulk counterpart, $T_f^0(x_{Kr})$. This result was expected since previous simulation [7, 31, 51–53] and theoretical [54–56] studies have shown that the freezing temperature of pure substances confined in a strongly attractive pore with $\alpha > 1$ is higher than the bulk value. An increase of the freezing temperature has also been observed in experiments for pure substances confined in strongly attractive pores such as cyclohexane between mica plates of the surface force apparatus [33, 34] or CCl_4 [35], CH_3OH [37], C_6H_6 [57] in activated carbon fibres.

3.1.2. *Freezing temperature and structure of the confined mixture*

In order to determine the freezing temperature of the Ar/Kr confined mixture we performed simulations at temperatures above the bulk freezing point. The constant parameters $\mu_{Ar}(T)$ and $\mu_{Kr}(T)$ in our simulations were determined as follows. For all temperatures T, the fugacities $f_i(T)$ of Ar and Kr were fixed equal to those for the bulk liquid/solid coexistence for our potential model $f_i(T_0)$ at a pressure of 1 atm:

$$f_i(T) = f_i(T_0), \quad i = \mathrm{Ar}, \mathrm{Kr}. \tag{11}$$

The different Ar and Kr constant fugacities conditions that were studied in this work are reported in table 3. For each set of fugacities, we carry out simulations for a range of temperatures; the temperature was varied by increments of $\Delta T = 2$ K over a range of several tens of kelvin. This choice of simulation conditions (choosing fugacities equal to those at the bulk mixture freezing point) avoids the problem of having to determine the chemical potentials in the bulk mixture at and near the pore freezing point [38]. However, the pressure of the bulk mixture will vary with the composition. We do not expect the pressure variation to have a large effect on the freezing phase diagram, as evidenced by previous results for the bulk mixtures [44]. Here we present, as an example, a detailed analysis of the results obtained for mixtures with fugacities $f_{Ar}^* = 1.91 \times 10^{-3}$ and $f_{Kr}^* = 6.36 \times 10^{-4}$ (in reduced units with respect to the Lennard–Jones parameters for Ar). The complete solid/liquid phase diagram (T, x_{Kr}) obtained from the analysis of the different fugacity conditions will be discussed at the end of this section.

In figure 6(*a*), we show the Kr mole fraction, x_{Kr}, of an Ar/Kr mixture with $f_{Ar}^* = 1.91 \times 10^{-3}$ and $f_{Kr}^* = 6.36 \times 10^{-4}$ for temperatures from 143.1 K up to 173.1 K, confined in the 1.44 nm slit graphite pore: $\alpha_{Ar} = 1.93$, $\alpha_{Kr} = 1.78$ and $\eta = 0.86$. Both data for the freezing and melting processes are reported. It is noteworthy that no hysteresis loop was observed between freezing and melting; the properties of the confined mixture x_{Kr}, Φ_6, $g(r)$, $G_6(r)$ are independent of the initial configuration, liquid-like or solid-like. As can be seen in figure 6(*a*), the Kr mole fraction slightly

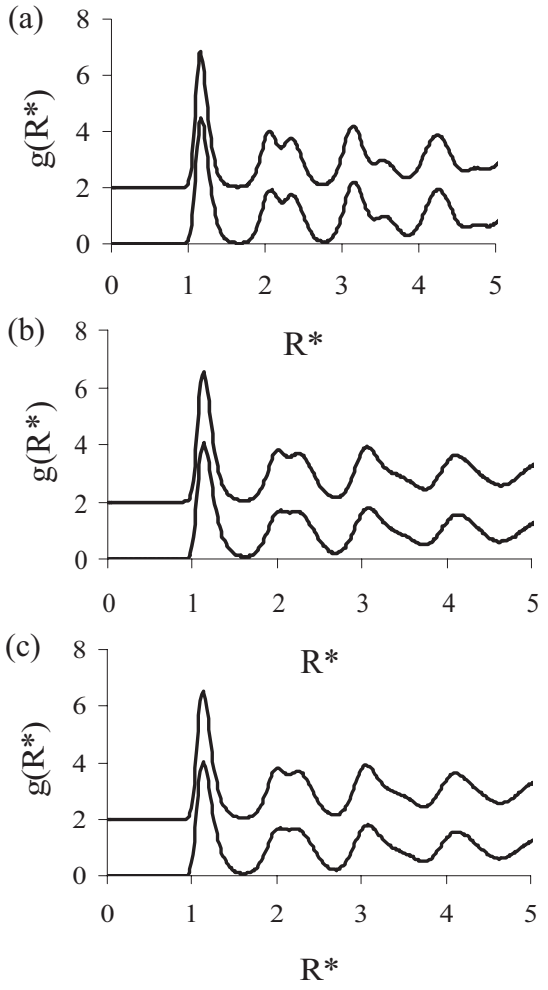

Figure 5. In-plane 2D pair correlation functions $g(r)$ for the contact and inner layers of Ar/Kr mixtures confined in the 1.44 nm slit pore, $\alpha_{Ar}=1.93$, $\alpha_{Kr}=1.78$, $\eta=0.86$, at different temperatures of the bulk solid/liquid coexistence: (*a*) $T=104.1$ K, (*b*) $T=97.9$ K and (*c*) 97.3 K. The Kr mole fraction inside the pore is (*a*) $x_{Kr}=0.82$, (*b*) $x_{Kr}=0.43$ and (*c*) $x_{Kr}=0.00$. For sake of clarity the $g(r)$ function corresponding to the contact layer has been shifted by $+2$. R^* is the distance in reduced units with respect to σ_{Ar}.

increases with decreasing temperature for temperatures above 153.1 K and below 151.1 K. In contrast, a sharp increase of x_{Kr} is observed at a temperature $T\sim 152.1$ K. This result suggests that structural changes in the confined mixture occur at this temperature. We show in figure 6 (*b*) the 2D order parameter Φ_6 for the contact and inner layers as a function of the temperature. The sudden change of Φ_6 with temperature confirms that both the contact and inner layers undergo a liquid-like to solid-like transition at a temperature $T_f\sim 152.1$ K (as will be seen below, an analysis of the pair correlation functions confirms that freezing occurs at this temperature). In the case of the contact layer, Φ_6 varies from

Table 3. Solid/liquid coexistence conditions for various Ar/Kr mixtures confined in a 1.44 nm slit pore with $\alpha_{Ar}=1.93$, $\alpha_{Kr}=1.78$, $\eta=0.86$, corresponding to the wall/fluid interactions parameters (A). f^*_{Ar} and f^*_{Kr} are the fugacities of Ar and Kr, respectively (reduced with respect to the Lennard–Jones parameters for Ar). T_f is the freezing temperature. x^C_{Kr} and x^L_{Kr} are the Kr mole fraction of the solid and liquid coexisting states, respectively. Bold data are results corresponding to the detailed analysis given in section 3.1.

f^*_{Ar}	f^*_{Kr}	T_f (K)	x^C_{Kr}	x^L_{Kr}
0.00	1.32×10^{-3}	159.9	1.00	1.00
1.91×10^{-3}	**6.36×10^{-4}**	**152.1**	**0.89**	**0.85**
2.39×10^{-3}	1.94×10^{-4}	139.6	0.71	0.64
1.77×10^{-3}	4.54×10^{-5}	127.1	0.54	0.46
1.61×10^{-3}	2.63×10^{-5}	122.0	0.45	0.38
1.44×10^{-3}	7.24×10^{-6}	114.9	0.21	0.18
1.20×10^{-3}	0.00	110.3	0.00	0.00

$\sim$0.15 in the liquid-like region up to $\sim$0.75 in the solid-like region. This latter value suggests that the contact layer has a hexagonal crystal structure with, however, a large number of defects. The variations of Φ_6 for the inner layer are very similar to those for the contact layer. However, Φ_6 for the contact layer is slightly larger than that for the inner layer at all temperatures. This result suggests that, due to the proximity of the pore wall, the contact layer is more ordered than the inner layer.

The sharp increase in the Kr mole fraction at the freezing temperature $T_f\sim 152.1$ K suggests that crystallization of the confined mixture is a first-order transition between two coexisting states having different molar compositions (see figure 6). This issue will be discussed in detail below. The Kr mole fractions of the coexisting liquid $x^L_{Kr}=0.85$ and crystal states $x^C_{Kr}=0.89$ at the freezing point were determined from the compositions of the Ar/Kr confined mixture at $T=153.1$ K and $T=151.1$ K, respectively (see figure 6 (*a*) and table 3). The freezing temperature $T_f=152.1$ K is much larger than the freezing point of a bulk mixture having a similar molar composition, $T_f^0\sim 125$ K (see figure 1), and corresponds to a relative increase T_f/T_f^0 of 1.22. The augmentation in the Kr mole fraction, upon solidification of the confined mixture, can be interpreted as follows. It corresponds to a decrease of the energy U of the system ($\varepsilon_{Kr}>\varepsilon_{Ar}$) that is needed to compensate the entropy loss S related to the transition from the liquid-like phase to the solid-like phase (given that the liquid-like and solid-like phases have the same free energy $A=U-TS$ at the freezing point). We note that a similar increase of the Kr mole fraction is also observed upon freezing of the bulk mixture (see figure 1).

The increase of freezing temperature that we observed for the confined Ar/Kr mixture is consistent with recent

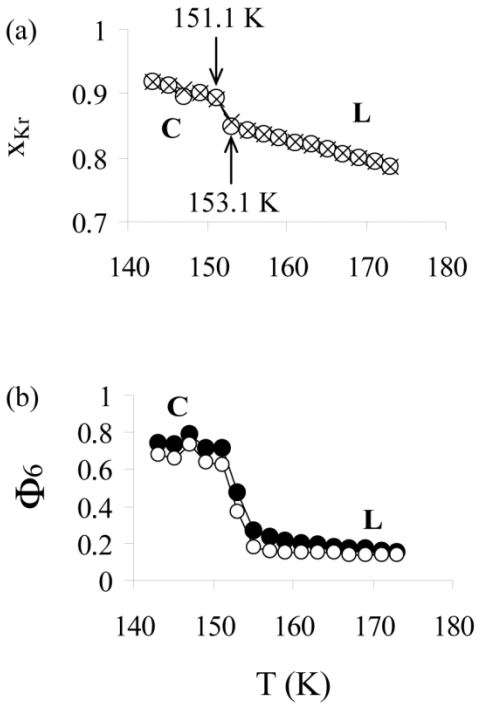

Figure 6. Freezing and melting of Ar/Kr mixtures confined in the 1.44 nm slit pore with $\alpha_{Ar} = 1.93$, $\alpha_{Kr} = 1.78$, $\eta = 0.86$, $f^*_{Ar} = 1.91 \times 10^{-3}$, $f^*_{Kr} = 6.36 \times 10^{-4}$ as a function of the temperature: (*a*) upon freezing starting with an initial composition $x_{Kr} \sim 0.79$ at $T = 173.1$ K (open circles); and upon melting starting with an initial composition $x_{Kr} \sim 0.92$ at $T = 143.1$ K (crosses). C and L denote the solid and liquid regions, respectively. (*b*) Variations upon freezing of the order parameter Φ_6 for the contact layer (closed circles) and the inner layer (open circles).

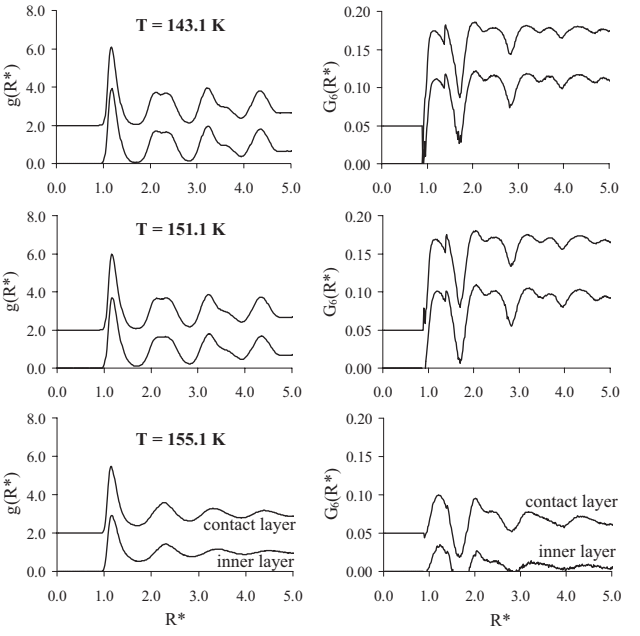

Figure 7. In-plane positional $g(r)$ and bond orientational $G_6(r)$ pair correlation functions for the contact and inner layers of an Ar/Kr mixture confined at four temperatures in the 1.44 nm slit pore, with $\alpha_{Ar} = 1.93$, $\alpha_{Kr} = 1.78$, $\eta = 0.86$. The Kr mole fraction of the confined mixture is $x_{Kr} \sim 0.92$ at $T = 143.1$ K, $x_{Kr} \sim 0.89$ at $T = 151.1$ K, $x_{Kr} \sim 0.84$ at $T = 155.1$ K. For the sake of clarity, the $g(r)$ and $G_6(r)$ functions for the contact layer have been shifted by $+2$ and $+0.05$, respectively. R^* is the distance in reduced units with respect to σ_{Ar}.

experimental results obtained by Sliwinska-Bartkowiak and coworkers for a carbon tetrachloride/cyclohexane mixture confined in activated carbon fibres [58]. Interestingly, the α parameters for this experimental system $\alpha_{CCl_4} = 1.93$, $\alpha_{C_6H_{12}} = 1.76$ are similar to those studied in the present work $\alpha_{Ar} = 1.93$, $\alpha_{Kr} = 1.78$ (in contrast, the parameters η are different). In the experimental study, the authors found that the freezing temperature for the CCl_4/C_6H_{12} confined mixture is 1.07 times larger than that for the bulk when the mole fraction of cyclohexane is about 0.8.

We now discuss the details of the structure of the Ar/Kr mixture confined in the 1.44 nm slit graphite pore. In-plane positional and bond orientational pair correlation functions of the confined Ar/Kr mixture, $f^*_{Ar} = 1.91 \times 10^{-3}$ and $f^*_{Kr} = 6.36 \times 10^{-4}$ are shown in figure 7 for several temperatures. Both the contact and the inner layers of the confined mixture have a solid-like structure at the two lowest temperatures $T = 143.1$ K and $T = 151.1$ K; the $g(r)$ function exhibits the solid-like features that have been described previously. In contrast, the positional pair correlation functions $g(r)$ at $T = 155.1$ K show that the contact and inner layers are liquid-like (no long range positional order). In the case of the solid-like phase at $T = 143.1$ K and 151.1 K, the constant value of $G_6(r)$ at large distances shows that the confined layers have a hexagonal crystal structure, in agreement with our previous conclusion. In contrast, the bond orientational pair correlation functions $G_6(r)$ obtained at $T = 155.1$ K decrease with the separation, as expected for non-crystalline layers (see the $g(r)$ functions for these temperatures). Due to the size of the simulation box $\sim 10\sigma$, the correlations could be measured up to a distance of 5σ which is insufficient to determine unambiguously whether the decay of $G_6(r)$ is algebraic (hexatic phase) or exponential (isotropic liquid phase). We note that the existence of a hexatic phase is expected according to the theory developed by Kosterlitz–Thouless–Halperin–Nelson–Young (KTHNY) for the melting of 2D systems [48, 59, 60]. Recently, Radhakrishnan *et al.* [61] have shown by means of GCMC simulations that the hexatic phase of Lennard–

Jones particles confined in strongly attractive pores is stable over a large range of temperatures. The authors have also obtained experimental results supporting the existence of such a hexatic phase for CCl_4 in activated carbon fibres [61]. Such experimental and simulation results suggest that hexatic phases may be observed for Ar/Kr mixtures confined in graphitic slit pores. On the other hand, the difference in size and interaction energy between the two components, Ar and Kr, might prevent the system from forming a hexatic phase. Further study including a system size scaling analysis [61] is needed to clarify this issue and check whether the confined mixture undergoes a crystal to hexatic phase transition followed by a hexatic to liquid phase transition or only a crystal to liquid phase transition. In what follows, the phase having no long range positional order will be systematically referred as liquid phase (L), but we acknowledge that an intermediate hexatic phase (H) may exist.

3.1.3. *Phase diagram of the confined mixture*

The coexistence conditions (T_f, x_{Kr}^{C}, x_{Kr}^{L}) for each set of parameters f_{Ar}^{*} and f_{Kr}^{*} are shown in table 3. These data were obtained following the analysis reported in the previous section; we determined upon freezing and melting the variations of x_{Kr} and Φ_6 with temperature. The structure of the confined mixture was studied for each temperature using both 2D positional $g(r)$ and bond orientational $G_6(r)$ pair correlation functions. Except for pure Kr, the freezing/melting process of the confined mixture was found to be reversible and the coexistence conditions, freezing temperature and molar compositions of the coexisting liquid and solid states, were determined unambiguously. In the case of pure Kr ($x_{Kr}=1.00$), a small hysteresis loop of $\Delta T=2\,K$ was observed and we defined the temperature of the solid/liquid transition $T_f=159.9\,K$ as the average value of the freezing temperature $T=158.9\,K$ and the melting temperature $T=160.9\,K$. We note that this approach gives a reasonable estimation of the transition temperature because of the very small width of the hysteresis loop. For the general case where wide hysteresis loops are observed, a free energy calculation is required to determine accurately the location of the transition.

The solid/liquid phase diagram obtained from the coexistence data for Ar/Kr mixtures confined in the 1.44 nm slit graphitic pore with $\alpha_{Ar}=1.93$, $\alpha_{Kr}=1.78$ and $\eta=0.86$ is shown in figure 8 (*a*). We have also reported the solid/liquid phase diagram obtained by Hitchcock and Hall for bulk Ar/Kr mixtures at $p=1$ atm [9]. The use of constant fugacities f_{Ar}^{*} and f_{Kr}^{*} in our study implies the equality of the chemical potentials and pressures at the freezing point T_f. On the other hand, it is worth mentioning that the coexistence data between the different sets of fugacities

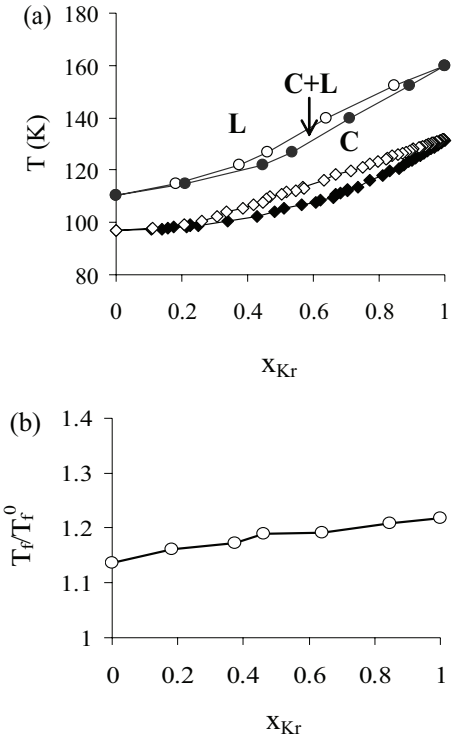

Figure 8. (*a*) (T, x_{Kr}) phase diagram of an Ar/Kr mixture confined in the 1.44 nm slit pore with $\alpha_{Ar}=1.93$, $\alpha_{Kr}=1.78$ and $\eta=0.86$. For each transition temperature T, open and closed circles indicate the Kr mole fraction of the coexisting liquid and crystal states, respectively. C and L denote the solid and liquid regions for the confined mixture, respectively. Open and closed diamonds indicate the solid/liquid coexistence lines for the bulk mixture (from Hitchcock and Hall [9]). (*b*) Ratio of the freezing temperature T_f for confined Ar/Kr mixtures with $\alpha_{Ar}=1.93$, $\alpha_{Kr}=1.78$, $\eta=0.86$ to that for the bulk mixture, T_f^0, as a function of the molar composition.

reported in table 3 do not correspond to the same pressure. Previous molecular simulations [62, 63] and experiments [64, 65] have shown that the in pore freezing temperature significantly depends on the pressure of the bulk reservoir. However, a comparison between our coexistence data for the freezing of confined Ar/Kr mixtures and the bulk data remains relevant since the bulk solid/liquid phase diagram is almost independent on the pressure [44]. Thus, we assume in what follows that the bulk phase diagram at pressures corresponding to our simulations is very nearly the same as that obtained by Hitchcock and Hall for a pressure $p=1$ atm. As can be seen in figure 8 (*a*), the phase diagram for the confined mixtures is of the same type as that for the bulk system, but the solid and liquid coexistence lines are located at higher temperatures. For each freezing temperature, the transition between the

liquid and crystal phases corresponds to a sharp increase of the Kr mole fraction (see figure 6). This result suggests that the liquid and crystal phases of the confined mixture coexist at the freezing point, i.e. the crystallization is a first order transition. In the case of pure Kr, this result is supported by the observation of a hysteresis loop associated with the existence of metastable states upon freezing and/or melting. However, further study including a free energy calculation [7, 31, 47] is required to establish in a rigorous way the order of the crystal to liquid phase transition when no hysteresis loop is observed.

The relative increase of the freezing temperature T_f/T_f^0 is shown in figure 8(*b*) as a function of the Kr mole fraction $x_{\mathrm{Kr}}^{\mathrm{L}}$. T_f/T_f^0 is a monotonic function of $x_{\mathrm{Kr}}^{\mathrm{L}}$, and increases from 1.14 for pure Ar up to 1.23 for pure Kr. Given that the α parameter is larger for Ar $\alpha_{\mathrm{Ar}} = 1.93$ than that for Kr $\alpha_{\mathrm{Kr}} = 1.78$, it is surprising to find the largest increase in freezing temperature for pure Kr. Indeed, previous simulation work has shown that the augmentation of the freezing temperature becomes larger as the parameter α increases, in agreement with experiments [7, 31]. One reason that may explain this result is that the reduced pore width for pure Kr, $H^* = 4.0$, is lower than that for pure Ar, $H^* = 4.3$. However, Radhakrishnan *et al.* [52] have shown that the freezing temperature of CCl_4 ($\alpha = 1.93$) confined in slit pores accommodating three layers is not very sensitive to the reduced pore width. In contrast, we have already mentioned that the freezing temperature of the confined system significantly depends on the pressure of the bulk reservoir [62–65]. The fact that the ratio of the freezing temperatures T_f/T_f^0 of pure Kr confined in the 1.44 nm slit pore is larger than that for pure Ar, may be an effect of varying pressure.

3.2. *Ar/Kr mixtures confined in a slit pore having a stronger affinity for Ar*

In this section, we study the freezing and melting of Ar/Kr mixtures confined in a 1.44 nm slit pore having a larger affinity for 'Ar' than for 'Kr', $\eta = \varepsilon_{\mathrm{Ar/W}}/\varepsilon_{\mathrm{Kr/W}} = 1.07$. These results were obtained using the wall/fluid energy parameters (B) corresponding to the following α parameters: $\alpha_{\mathrm{Ar}} = 2.40$ and $\alpha_{\mathrm{Kr}} = 1.78$. As in the case of the set of wall/fluid interactions (A), the freezing of Ar/Kr mixtures confined in the 1.44 nm slit pore was studied for different constant values of f_{Ar}^* and f_{Kr}^* (see table 4). The analysis of the results was carried out as explained in the previous section, except that we did not simulate the melting process in every case. However, in all cases where both freezing and melting were studied ($x_{\mathrm{Kr}} \sim 0.00$, 0.13, 0.30, 0.50, 0.60 and 0.90), the transition was found to be reversible. Moreover, results obtained in the first part of this work (section 3.1) suggest that the melting data are not crucial in this study since very small ($\Delta T = 2$ K) or no hysteresis loop was observed. Here we present details of our results for two confined mixtures, one that is rich in Kr, $x_{\mathrm{Kr}} \sim 0.9$, and one rich in Ar, $x_{\mathrm{Kr}} \sim 0.15$. Simulations for the mixture having a high Kr molar concentration were carried out for temperatures in the range 136–166 K at constant fugacities $f_{\mathrm{Ar}}^* = 6.63 \times 10^{-4}$ and $f_{\mathrm{Kr}}^* = 1.10 \times 10^{-3}$. Data for the mixture with the low Kr mole fraction were obtained for various temperatures in between 110 and 140 K, at constant fugacities $f_{\mathrm{Ar}}^* = 1.77 \times 10^{-3}$ and $f_{\mathrm{Kr}}^* = 4.54 \times 10^{-5}$. The complete solid/liquid phase diagram (T, x_{Kr}) obtained from the analysis of the different fugacities conditions will be discussed at the end of this section.

The 2D order parameters Φ_6 for each confined mixture, $x_{\mathrm{Kr}} \sim 0.90$, and $x_{\mathrm{Kr}} \sim 0.15$, are presented

Table 4. Solid/liquid coexistence conditions for various Ar/Kr mixtures confined in a 1.44 nm slit pore with $\alpha_{\mathrm{Ar}} = 2.40$, $\alpha_{\mathrm{Kr}} = 1.78$, $\eta = 1.07$, corresponding to the wall/fluid interactions parameters (B). f_{Ar}^* and f_{Kr}^* are the fugacities of Ar and Kr, respectively (reduced with respect to the Lennard–Jones parameters for Ar). For Kr mole fractions larger than 0.35, both the contact and the inner layers freeze at the temperature $T_{\mathrm{L/C}}$. For Kr mole fractions smaller than 0.35, the contact and inner layers crystallize at different temperatures $T_{\mathrm{L/CC}}$ and $T_{\mathrm{CC/C}}$. $T_{\mathrm{L/CC}}$ is the temperature of the transition between the liquid and the contact-crystal and $T_{\mathrm{CC/C}}$ is the temperature of the transition between the contact-crystal phase and the crystal. In each case, x_{Kr}^1 and x_{Kr}^2 are the molar composition of the coexisting states having a high and low Kr mole fraction, respectively. Bold data are results corresponding to the detailed analysis given in section 3.2.

f_{Ar}^*	f_{Kr}^*	$T_{\mathrm{L/C}}$ or $T_{\mathrm{L/CC}}$ (K)	x_{Kr}^1	x_{Kr}^2	$T_{\mathrm{CC/C}}$ (K)	x_{Kr}^1	x_{Kr}^2
0.00	1.32×10^{-3}	159.9	1.00	1.00	—	—	—
6.63×10^{-4}	**1.10×10^{-3}**	**157.0**	**0.91**	**0.86**	—	—	—
1.91×10^{-3}	6.36×10^{-4}	144.1	0.66	0.60	—	—	—
2.22×10^{-3}	4.70×10^{-4}	139.0	0.57	0.50	—	—	—
2.30×10^{-3}	4.05×10^{-4}	137.0	0.49	0.46	—	—	—
2.42×10^{-3}	2.69×10^{-4}	133.0	0.40	0.36	—	—	—
2.39×10^{-3}	1.94×10^{-4}	130.6	0.30	0.30	128.6	0.31	0.30
1.77×10^{-3}	**4.54×10^{-5}**	**128.0**	**0.13**	**0.13**	**123.0**	**0.15**	**0.15**
1.20×10^{-3}	0.00	128.3	0.00	0.00	114.3	0.00	0.00

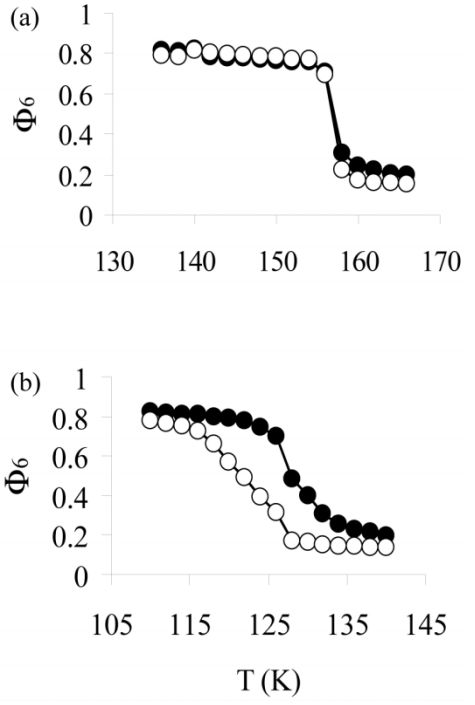

Figure 9. (*a*) Order parameter Φ_6 for the contact layer (closed circles) and the inner layer (open circles) of an Ar/Kr mixture with $x_{Kr} \sim 0.90$ confined in a 1.44 nm slit pore with $\alpha_{Ar} = 2.40$, $\alpha_{Kr} = 1.78$, $\eta = 1.07$, as a function of the temperature (upon freezing). (*b*) Same as (*a*) for an Ar/Kr confined mixture having a Kr mole fraction $x_{Kr} \sim 0.15$.

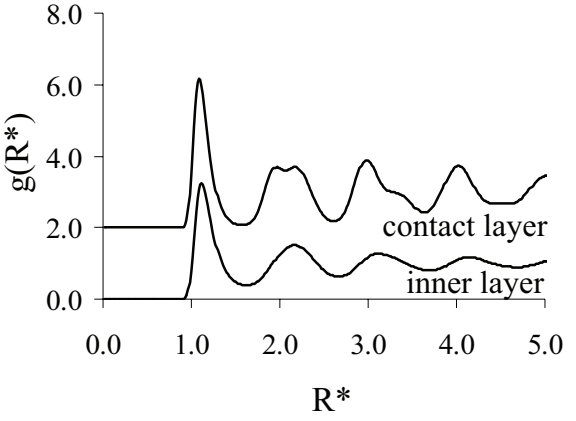

Figure 10. n-plane positional $g(r)$ for the contact and inner layers of an Ar/Kr mixture confined at $T = 124.0$ K in a 1.44 nm slit pore with $\alpha_{Ar} = 2.40$, $\alpha_{Kr} = 1.78$ and $\eta = 1.07$. The Kr mole fraction of the confined mixture is $x_{Kr} \sim 0.15$. For the sake of clarity, the $g(r)$ function for the contact layer has been shifted by $+2$. R^* is the distance in reduced units with respect to σ_{Ar}.

in figure 9 as a function of the temperature. Data for the contact and the inner layers are reported. In the case of the mixture rich in Kr, we found that the inner and contact layers crystallize at the same temperature $T_f = 157.0$ K (see figure 9 (*a*)). The freezing behaviour for this confined mixture $x_{Kr} \sim 0.90$ is similar to that observed in the previous section when interaction parameters (A) were used. In contrast, results for the mixture $x_{Kr} \sim 0.15$ show that the contact and the inner layer crystallize at different temperatures, $T = 128.0$ K and $T = 123.0$ K, respectively. This result is supported by the positional $g(r)$ functions at the intermediate temperature $T = 124.0$ K (see figure 10): the inner layer has a liquid-like structure while the contact layer has a solid-like structure. We note that this phase, consisting of a crystal contact layer and a liquid-like inner layer, has already been observed by Radhakrishnan *et al.* [7, 31] in the case of pure methane confined in a slit graphite pore with $\alpha = 2.16$, $H^* = 7.5$. Following these previous works, we term this new phase 'contact-crystal'. For both the liquid (L) to contact-crystal (CC) and crystal-contact to crystal (C) phase transitions, we determined the Kr mole fraction of the Ar/Kr mixture at the transition temperatures $T_{L/CC} = 128.0$ K and $T_{CC/C} = 123.0$ K (see table 4).

The solid/liquid phase diagram (T, x_{Kr}) for confined Ar/Kr mixtures corresponding to the interaction parameters (B) is compared in figure 11 (*a*) with results obtained by Hitchcock and Hall for bulk Ar/Kr mixtures [9]. For Kr mole fractions larger than 0.35, the confined mixture undergoes a liquid to crystal transition upon freezing, and no intermediate contact-crystal phase is observed. In contrast, confined mixtures having a Kr mole fraction lower than 0.35 first undergo a liquid to contact-crystal phase transition, followed by a contact-crystal to crystal phase transition. In the case of the crystal to liquid phase transition ($x_{Kr} > 0.35$), our results suggest that the transition is first order since the transformation involves a sudden change in the molar composition of the mixture (see table 4). As a result, we report in the phase diagram shown in figure 11 the Kr mole fraction of both the liquid and crystal phases. In contrast, we were not able to distinguish any sharp change in the Kr mole fraction upon the CC to C or L to CC phase transitions ($x_{Kr} < 0.35$). This result suggests that these phase transitions are either second order or weakly first order. Consequently, the CC/C and L/CC phase transitions in the solid/liquid phase diagram shown in figure 11 appear as lines rather than coexistence loops. Again, free energy calculations would allow us to clarify this issue and determine unambiguously the nature of the solid/liquid phase transitions in the different situation $x_{Kr} > 0.35$ or < 0.35.

We note that the contact-crystal region was not observed for confined mixtures with $\alpha_{Ar} = 1.93$, corresponding to wall/fluid interactions (A), but only with

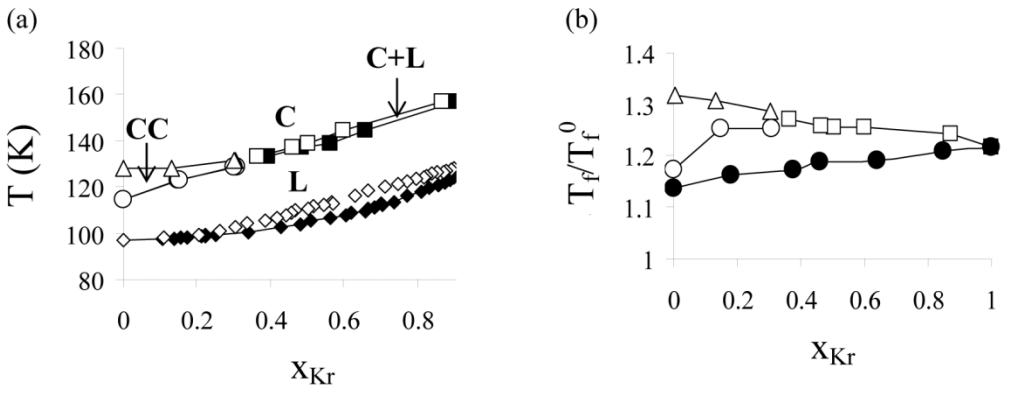

Figure 11. (*a*) (T, x_{Kr}) phase diagram of an Ar/Kr mixture confined in a 1.44 nm slit graphitic pore with $\alpha_{Ar} = 2.40$, $\alpha_{Kr} = 1.78$ and $\eta = 1.07$. Open and closed squares are the coexistence conditions corresponding to the liquid to crystal phase transition ($x_{Kr} > 0.35$). Circles and triangles are respectively data for the contact-crystal to crystal and the liquid to contact-crystal phase transitions ($x_{Kr} < 0.35$). For these two phase transitions the mole fractions of the coexisting phases are almost the same (see table 4) and cannot be distinguished on the scale of the plot. Open and closed diamonds indicate the solid/liquid coexistence lines for the bulk mixture (from Hitchcock and Hall [9]). C, L and CC denote the crystal, liquid and contact-crystal regions for the confined mixture, respectively. (*b*) Ratio of the freezing temperature for confined Ar/Kr mixtures ($\alpha_{Ar} = 2.40$, $\alpha_{Kr} = 1.78$, $\eta = 1.07$, T_f, to that for the bulk mixture, T_f^0, as a function of the molar composition. Squares are the freezing temperatures corresponding to the liquid to crystal phase transition ($x_{Kr} > 0.35$). Triangles and open circles are, respectively, the transition temperatures of the liquid to contact-crystal and contact-crystal to crystal phases ($x_{Kr} < 0.35$). Black circles are the freezing temperatures for the confined Ar/Kr mixtures with $\alpha_{Ar} = 1.93$, $\alpha_{Kr} = 1.78$ and $\eta = 0.86$.

$\alpha_{Ar} = 2.40$, corresponding to parameters (B). This significant effect of the α parameter on the phase diagram of the confined mixture contrasts with previous simulation results obtained for the freezing of pure substances confined in a strongly attractive slit pore ($\alpha > 1$) [7, 31]. In these studies, Radhakrishnan *et al.* have shown that contact-crystal phases were always observed provided that α was larger than 1. However, these results were obtained for a pore width $H^* = 7.5$ (with five inner layers), much larger than that used in our study $H^* \sim 4$ (with one inner layer). One may expect the contact-crystal phase to be more stable for large pore widths due to the important difference in wall/fluid interactions between the contact and the inner layers.

We show in figure 11 (*b*) the ratio of the transition temperature for the confined mixture, $\alpha_{Ar} = 2.40$, with the bulk freezing point T_f^0 as a function of the molar composition. For Kr mole fraction smaller than 0.35, both data for the crystal to contact-crystal transition $T_{CC/C}$ and the liquid to contact-crystal transition $T_{L/CC}$ are reported. For Kr mole fractions larger than 0.35, we present the results for the liquid to crystal transition $T_{L/C}$. Finally, we also show in figure 11 (*b*) the results obtained in section 3.1 for Ar/Kr mixtures corresponding to wall/fluid interactions (A), $\alpha_{Ar} = 1.93$. The transition temperatures $T_{L/C}$ ($x_{Kr} > 0.35$) and $T_{L/CC}$ ($x_{Kr} < 0.35$) of the confined mixtures with wall/fluid interactions (B) are larger than the bulk freezing temperature T_f^0 for all molar compositions. This result was expected since the values $\alpha_{Ar} = 2.40$ and $\alpha_{Kr} = 1.78$ are much larger than 1. The transition temperature $T_{CC/C}$ ($x_{Kr} < 0.35$) is also located at higher temperatures than the bulk freezing temperature. As expected, the freezing temperature of the contact layer, $T_{L/C}$ or $T_{L/CC}$, and of the inner layer, $T_{L/C}$ or $T_{CC/C}$, for Ar/Kr mixtures having the largest $\alpha_{Ar} = 2.40$ are significantly higher than those for mixtures corresponding to $\alpha_{Ar} = 1.93$.

The relative increase of freezing temperature $T_{L/C}$ and $T_{L/CC}$ for the contact layer of mixtures with $\alpha_{Ar} = 2.40$ is a decreasing function of the Kr mole fraction from 1.32 for pure Ar down to 1.22 for pure Kr. This decreasing behaviour of the function $T_f/T_f^0(x_{Kr})$ differs from the increasing behaviour that is observed for confined Ar/Kr mixtures with $\alpha_{Ar} = 1.93$. This result suggests that the qualitative variations of the freezing temperature with the molar composition of the confined mixture depends on the ratio $\eta = \varepsilon_{Ar/W}/\varepsilon_{Kr/W}$, rather than on the α parameter. Indeed, the η parameters for the two types of confined Ar/Kr mixtures are significantly different, $\eta = 0.86$ (A) and 1.07 (B), and correspond to pore walls having either a stronger affinity for Kr or for Ar. As observed in our simulations, one may expect the freezing temperature to increase with increasing mole fraction of the component having the stronger wall/fluid interaction increases. Further study is needed to clarify this issue and check the effect of the parameter η on the freezing and melting of the confined mixture.

4. Conclusions

In this paper, we use Grand Canonical Monte Carlo simulations to study the freezing of Lennard–Jones Ar/Kr mixtures confined in a structureless slit pore

composed of two strongly attractive walls, with α_{Ar} and $\alpha_{Kr} > 1$. For all molar compositions and temperatures, the pore of width 1.44 nm accommodates two contact layers and one inner layer. We consider different wall/fluid interactions corresponding to strongly attractive pore walls, having either a larger affinity for Ar, $\eta = \varepsilon_{Ar/W}/\varepsilon_{Kr/W} = 1.07$, or Kr, $\eta = 0.86$. The structure of the confined mixture is determined by calculating for each layer 2D bond order parameters, Φ_6, and both positional $g(r)$ and bond orientational $G_6(r)$ pair correlation functions. For the different wall/fluid interactions, we discuss the confinement effect on the freezing temperature and its dependence on the molar composition of the mixture. We also determine the solid/liquid phase diagram of the confined system and compare our results with experimental and theoretical data available for the bulk mixture.

As expected for strongly attractive pores, we show that the freezing point of the Ar/Kr confined mixture is higher than the bulk freezing point for all molar compositions. This result is in qualitative agreement with recent experimental results obtained by Sliwinska-Bartkowiak and coworkers [58] for a carbon tetrachloride/cyclohexane mixture confined in activated carbon fibres. We also find that the freezing temperature of the Ar/Kr confined mixture becomes higher as the α parameter increases, in agreement with previous simulations studies for pure substances confined in nanopores. In the case of pore walls having a stronger affinity for Kr atoms ($\eta = \alpha_{Ar} = 1.93$, $\alpha_{Ar} = 1.78$), we observe that both the contact and inner layers of the confined mixture undergo, at the same temperature, a transition from the liquid phase to the crystal phase. At the freezing point, we find that the Kr mole fraction sharply increases, which suggests that there is coexistence of liquid and solid phases having different molar compositions (first order phase transition). It is shown that the confined solid mixture is composed of 2D crystal layers having a hexagonal structure. For temperatures above the freezing point, it is not clear whether the confined mixture undergoes a crystal to hexatic phase transition followed by a hexatic to liquid phase transition or directly a crystal to liquid phase transition. Further calculations for larger system sizes are needed to clarify this issue.

The freezing of Ar/Kr mixtures confined within the walls having a stronger affinity for Ar atoms ($\eta = 1.07$, $\alpha_{Ar} = 2.40$, $\alpha_{Ar} = 1.78$) is more complex. For Kr mole fractions larger than 0.35, the freezing behaviour of the confined mixtures is similar to that observed for the mixture ($\eta = 0.86$, $\alpha_{Ar} = 1.93$, $\alpha_{Ar} = 1.78$). In contrast, results obtained for confined mixtures $\eta = 1.07$ having a Kr molar concentration lower than 0.35 show the presence of an intermediate contact layer crystal phase between the hexagonal crystal phase and the liquid phase. This intermediate phase consists of a crystalline contact layer and a liquid-like inner layer. Our results suggest that the transition between the crystal/contact-crystal and contact-crystal/liquid phases are either second order or weakly first order transitions. This result departs from what is observed for mixtures that undergo a direct crystal to liquid phase transition ($x_{Kr} > 0.35$). It is noteworthy that these conclusions are based on the changes in the 2D order parameters and the Kr mole fraction with temperature. A free energy calculation is required to determine the order of the phase transitions in a rigorous way.

The dependence of the freezing temperature on the molar composition of the confined mixtures with $\eta = 1.07$ also strongly departs from that observed for $\eta = 0.86$. In the case $\eta = 1.07$, the relative increase of freezing temperature for the L/CC transition is a monotonically decreasing function of the Kr mole fraction while the opposite trend is observed for the L/C transition for mixtures corresponding to $\eta = 0.86$. These results suggest that the variations of the freezing temperature with the molar composition of the confined mixture depends on the affinity of the pore wall for the components Ar and Kr *via* the parameter $\eta = \varepsilon_{Ar/W}/\varepsilon_{Kr/W}$.

We are grateful to Carol K. Hall, Henry Bock and Erik Santiso (North Carolina State University) and to Ravi Radhakrishnan (New York University) for helpful discussions and comments. We also thank Brian C. Attwood and Monica H. Lamm for providing useful data. This work was supported by the Petroleum Research Fund of the American Chemical Society and by the Polish Science Foundation (*Komitet Badan Naukowych*). Supercomputing time was provided by the National Partnership for Advanced Computational Infrastructure (NPACI – NPA 205). International cooperation was supported by a NATO Collaborative Linkage Grant (No. PST.CLG.978802).

References

[1] Gelb, L. D., Gubbins, K. E., Radhakrishnan, R., and Sliwinska-Bartkowiak, M., 1999, *Rev. Prog. Phys.*, **62,** 1573.
[2] Christenson, H. K., 2001, *J. Phys.: Condens. Matter*, **13,** 95.
[3] Alba-Simionesco, C., Coasne, B., Dosseh, G., Dudziak, G., Gubbins, K. E., Radhakrishnan, R., and Sliwinska-Bartkowiak, M., *J. Phys.: Condens. Matter* (to be published).
[4] Meyer, R. R., Sloan, J., Dunin-Borkowski, R. E., Kirkland, A. I., Novotny, M. C., Bailey, S. R., Hutchison, J. L., and Green, L. M. H., 2000, *Science*, **289,** 1324.
[5] Wilson, M., 2002, *J. Chem. Phys.*, **116,** 3027.

[6] Cui, B., Lin, B., and Rice, S., 2003, *J. Chem. Phys.* **119,** 2386.
[7] Radhakrishnan, R., Gubbins, K. E. and Sliwinska-Bartkowiak, M., 2002, *J. Chem. Phys.*, **116,** 1147.
[8] Heastie, R., 1955, *Nature (London)*, **176,** 747.
[9] Hitchcock, M. R., and Hall, C. K., 1999, *J. Chem. Phys.*, **110,** 11433.
[10] Powles, J. G., 1994, *Philos. Mag.* B, **69,** 989.
[11] Calleja, M., North, A. N., Powles, J. G., and Rickayzen, G., 1991, *Mol. Phys.* **73,** 973.
[12] Powles, J. G., Rickayzen, G., and Williams, M. L., 1988, *Mol. Phys.*, **64,** 33.
[13] Murad, S., Ravi, P., and Powles, J. G., 1993, *J. Chem. Phys.*, **98,** 9771.
[14] Powles, J. G., Murad, S., and Ravi, P. V., 1992, *Chem. Phys. Lett.*, **188,** 21.
[15] Smith, D. W. G., 1966, Thesis 'Proton magnetic resonance in deuterated liquid mixtures', Queen Mary College, London University.
[16] Baharudin, B. Y., 1974, Thesis 'Brillouin scattering in the rare gas liquids and some mixtures of the rare gases', Queen Mary College, London University.
[17] Holtz, B., 1996, Thesis 'Investigations of Lennard–Jones fluids and their binary mixtures by simulation and theory', Queen Mary College, London University.
[18] Powles, J. G., and Pajak, Z., 1964, *Mol. Phys.*, **7,** 579.
[19] Nicholson, D., and Parsonage, N. G., 1982, *Computer Simulation and the Statistical Mechanics of Adsorption* (London: Academic Press).
[20] Allen, M. P., and Tildesley, D. J., 1987, *Computer Simulation of Liquids* (Oxford: Clarendon Press).
[21] Frenkel, D., and Smit, B., 2002, *Understanding Molecular Simulation*, 2nd edn (New York: Academic Press).
[22] Cracknell, R. F., Nicholson, D., and Quirke, N., 1993, *Mol. Phys.*, **80,** 885.
[23] Yan, Q. L., and de Pablo, J. J., 1999, *J. Chem. Phys.*, **111,** 9509.
[24] Faller, R., Yan, Q. L. and de Pablo, J. J., 2002, *J. Chem. Phys.*, **116,** 5419.
[25] Marinari, E., and Parisi, G., 1992, *Europhys. Lett.*, **191,** 451.
[26] Yan, Q. L. and de Pablo, J. J., 2000, *J. Chem. Phys.*, **113,** 1276.
[27] Clifford, A. A., Gray, P., and Platts, N., 1977, *J. Chem. Soc. Faraday Trans.*, **173,** 381.
[28] Rowlinson, J. S., 1982, *Liquids and Liquid Mixtures* (London: Butterworth Scientific).
[29] Steele, W. A., 1973, *Surf. Sci.*, **36,** 317.
[30] Steele, W. A., 1974, *The Interaction of Gases with Solid Surfaces* (Oxford: Pergamon Press).
[31] Radhakrishnan, R., Gubbins, K. E. and Sliwinska-Bartkowiak, M., 2000, *J. Chem. Phys.*, **112,** 11048.
[32] Reed, T. M., and Gubbins, K. E., 1973, *Applied Statistical Mechanics* (New York: McGraw Hill).
[33] Klein, J., and Kumacheva,, E., 1995, *Science*, **269,** 816.
[34] Klein, J., and Kumacheva,, E., 1998, *J. Chem. Phys.* **108,** 6996.
[35] Kaneko, K., Watanabe, A., Iiyama, T., Radhakrishan, R., and Gubbins, K. E., 1999, *J. Chem. Phys. B*, **103,** 7061.
[36] Watanabe, A., and Kaneko, K., 1999, *Chem. Phys. Lett.*, **305,** 71.
[37] Sliwinska-Bartkowiak, M., Dudziak, G., Sikorski, R., Gras, R., Gubbins, K. E., and Radhakrishnan, R., *Phys. Chem. Chem. Phys.*, **3,** 1179.
[38] Miyahara, M., and Gubbins, K. E., 1997, *J. Chem. Phys.*, **106,** 2865.
[39] Kofke, D. A., 1993, *Mol. Phys.*, **78,** 1331.
[40] Kofke, D. A., 1993, *J. Chem. Phys.*, **98,** 4149.
[41] Kofke, D. A., 1998, *Monte Carlo Methods in Chemistry*, edited by D. M. Ferguson, J. I. Siepmann and D. G. Truhlar (New York: Interscience).
[42] Lamm, M. H., and Hall, C. K., 2001, *Fluid Phase Equilibria*, **182,** 37.
[43] Lamm, M. H., and Hall, C. K., 2001, *AIChE J.*, **47,** 1664.
[44] Lamm, M. H., and Hall, C. K., 2002, *Fluid Phase Equilibria*, **194–197,** 197.
[45] Mehta, M., and Kofke, D. A., 1994, *Chem. Eng. Sci.*, **49,** 2633.
[46] Press, W. H., Teukolsky, S. A. Vetterling, W. T., and Flannery, B. P., 1992, *Numerical Recipes in Fortran 77 : the Art of Scientific Computing*, 2nd edn (Cambridge: Cambridge University Press).
[47] Radhakrishnan, R. and Gubbins, K. E., 1999, *Mol. Phys.*, **96,** 1249.
[48] Strandburg, K. J., 1988, *Rev. Mod. Phys.*, **60,** 161.
[49] Tan, Z., and Gubbins, K. E., 1992, *J. Phys. Chem.*, **96,** 845.
[50] Ayappa, K. G., and Ghatak, C., 2002, *J. Chem. Phys.*, **117,** 5373.
[51] Miyahara, M., and Gubbins, K. E. , *J. Chem. Phys.* **106,** 2865 (1997).
[52] Radhakrishnan, R., Gubbins, K. E., Watanabe, A., and Taneko, K., 1999, *J. Chem. Phys.*, **111,** 9058.
[53] Maddox, M. W., and Gubbins, K. E., 1997, *J. Chem. Phys.*, **107,** 9659.
[54] Tkatchenko, A., and Rabin, Y., 1997, *Solid State Commun.*, **103,** 361.
[55] Tkatchenko, A., and Rabin, Y., 1997, *Langmuir*, **13,** 7146.
[56] Weinstein, A., and Safran, S., 1998, *Europhys. Lett.*, **42,** 61.
[57] Watanabe, A., and Kaneko, K., 1999, *Chem. Phys. Lett.*, **305,** 71.
[58] Sliwinska-Bartkowiak, M. *et al.*, in preparation.
[59] Kosterlitz, J. M., and Thouless, D. J., 1972, *J. Phys. C*, **5,** L124; 1973, *J. Phys. C*, **6,** 1181.
[60] Halperin, B. I., and Nelson, D. R., 1978, *Phys. Rev. Lett.*, **41,** 121; Nelson, D. R., and Halperin, B. I., 1979, *Phys. Rev. B*, **19,** 2457; Young, A. P., 1979, *Phys. Rev. B*, **19,** 1855.
[61] Radhakrishnan, R., Gubbins, K. E., and Sliwinska-Bartkowiak, M., 2002, *Phys. Rev. Lett.*, **89,** 076101.
[62] Dominguez, H., Allen, M. P., and Evans, R., 1999, *Mol. Phys.*, **96,** 209.
[63] Miyahara, M., Kanda, H., Shibao, M., and Higashitani, K., 2000, *J. Chem. Phys.*, **112,** 9909.
[64] Duffy, J. A., Wilkinson, N. J., Fretwell, H. M., Alam, M. A., and Evans, R., 1995, *J. Phys. Condens. Matte*r, **7,** L713.
[65] Duffy, J. A., and Alam, M. A., 2000, *Langmuir*, **16,** 9513.